Available online at www.sciencedirect.com
ScienceDirect
Journal of Sound and Vibration 321 (2009) 936–954
JOURNAL OF SOUND AND VIBRATION
www.elsevier.com/locate/jsvi

Thermal effects on geometrically nonlinear vibrations of rectangular plates with fixed edges

M. Amabili*, S. Carra

Dipartimento di Ingegneria Industriale, Università di Parma, Viale Usberti 181/A, Parma 43100, Italy

Received 24 June 2008; received in revised form 30 September 2008; accepted 6 October 2008
Handling Editor: M.P. Cartmell
Available online 22 November 2008

Abstract

Nonlinear forced vibrations and postbuckling of isotropic rectangular plates subjected to thermal variations are studied. Geometric imperfections are taken into account since they play a fundamental role. The plate is modelled by using the Von Kármán hypothesis and the equations of motion are obtained by using an energy approach. Plates with fixed edges and additional rotational elastic constraint are considered. A pseudo-arclength continuation method is used in order to obtain numerical results. Laboratory experiments have been performed on two plates of different thickness.

1. Introduction

Geometrically nonlinear vibrations (also referred to as large-amplitude vibrations) arise when the vibration amplitude is of the order of the plate thickness. For perfectly flat plates with fixed edges, a strong hardening type nonlinearity is obtained [1]. However, geometric imperfections may cause the plate to deviate for the ideal configuration taking a small initial curvature, which may cause an initial softening type nonlinearity, turning to hardening type for larger amplitudes [1].

The study of nonlinear vibration of plates is introduced in the books of Amabili [1] and Chia [2]. Reviews of studies on nonlinear vibrations of plates were written by Sathyamoorthy [3] and Chia [4]. The pioneers in this area were Chu and Herrmann [5]. They studied simply supported rectangular plates with immovable edges and obtained the free vibration curve (also known as the backbone curve) for the fundamental mode of rectangular plates with different aspect ratios. The solution was obtained by using a perturbation procedure and shows strong hardening type nonlinearity.

The literature presents a large number of studies dealing with different boundary conditions, different solution methods and complicating effects [6–19]. Even if a large number of theoretical studies on large-amplitude vibrations of plates are available in the scientific literature, experimental results are very scarce. Complete experimental results are given by Amabili [13,14], and only experimental mode shapes for vibration

*Corresponding author. Tel.: +39 0521 905896; fax: +39 0521 905705.
E-mail address: marco.amabili@unipr.it (M. Amabili).
URL: http://me.unipr.it/mam/amabili/amabili.html (M. Amabili).

0022-460X/$ - see front matter © 2008 Elsevier Ltd. All rights reserved.
doi:10.1016/j.jsv.2008.10.004

amplitude 0.5 and 0.8 times the plate thickness are given by Harras et al. [15] for the fundamental mode of a clamped laminated rectangular plate.

Thermal variations with respect to the assembly temperature of fixed plates may introduce very large thermal stresses in plates since they are flat and they cannot expand due to the boundary conditions. Plates with fixed edges may buckle due to small thermal variations. Girish and Ramachandra [20] investigated the postbuckling and the postbuckled linear (small-amplitude) vibrations of rectangular plates with initial geometric imperfections. Lee and Reddy [21] analysed the transient nonlinear response of laminated composite plates under thermomechanical loading. Ribeiro [22] studied nonlinear vibrations of rectangular plates under thermal loads. Ribeiro and Jansen [23] and Librescu and Lin [24] extended the study to shells. Nonlinear vibrations of rectangular functionally graded plates under thermal variations were studied by Praveen and Reddy [25], Yang et al. [26], Huang and Shen [27], Park and Kim [28] and Woo et al. [29]. The temperature effect on circular and skew functionally graded plates was investigated by Allahverdizadeh et al. [30] and Sundararajan et al. [31], respectively. In general, these studies on nonlinear vibrations of thermally loaded plates are limited to free vibrations, to transient analysis or to response to harmonic excitation at fixed excitation frequency. A study on the thermal effect on large amplitude vibrations of Timoshenko beams is due to Manoach and Ribeiro [32].

In the present study, nonlinear forced vibrations and postbuckling of isotropic rectangular plates subjected to thermal variations are studied in the frequency range around the first resonace. Geometric imperfections are taken into account since they play a fundamental role. The plate is modelled by using the Von Kármán hypothesis and the equations of motion are obtained by using an energy approach. A pseudo-arclength continuation method is used in order to obtain numerical results. Laboratory experiments have been performed to support the numerical results.

2. Theory

A rectangular isotropic plate of uniform thickness h and in-plane dimensions a and b is assumed. A rectangular coordinate system (O; x, y, z) is introduced, where the origin O is assumed at a plate corner on the middle plane of the plate, x and y are the in-plane coordinates and z is the out-of-plane coordinate. At each point of the middle surface of the plate, the displacements in the x, y, z directions are denoted by u, v, w, respectively. Shear deformation and rotary inertia are neglected since for thin plates (and also for moderately thick plates in case of isotropic material) their contribution is fully irrelevant, as shown in Ref. [33]. The strain components ε_{xx}, ε_{yy} and γ_{xy} at an arbitrary point of the plate are related to the middle surface strains $\varepsilon_{x,0}$, $\varepsilon_{y,0}$ and $\gamma_{xy,0}$ and to the changes in the curvature and torsion of the middle surface k_x, k_y and k_{xy} by the following three relations [1]:

$$\varepsilon_{xx} = \varepsilon_{x,0} + zk_x, \tag{1}$$

$$\varepsilon_{yy} = \varepsilon_{y,0} + zk_y, \tag{2}$$

$$\gamma_{xy} = \gamma_{xy,0} + zk_{xy}, \tag{3}$$

where z is, as usual, the distance of the arbitrary point of the plate from the middle surface. Initial geometric imperfections of the rectangular plate associated with zero initial stress are denoted by normal displacement w_0; in-plane initial imperfections are neglected. If Von Kármán hypothesis is used, the following expressions for the middle surface strains and the changes in the curvature and torsion of the middle surface are obtained, namely Ref. [1]

$$\varepsilon_{x,0} = \frac{\partial u}{\partial x} + \frac{1}{2}\left(\frac{\partial w}{\partial x}\right)^2 + \frac{\partial w}{\partial x}\frac{\partial w_0}{\partial x}, \tag{4}$$

$$\varepsilon_{y,0} = \frac{\partial v}{\partial y} + \frac{1}{2}\left(\frac{\partial w}{\partial y}\right)^2 + \frac{\partial w}{\partial y}\frac{\partial w_0}{\partial y}, \tag{5}$$

$$\gamma_{xy,0} = \frac{\partial u}{\partial y} + \frac{\partial v}{\partial x} + \frac{\partial w}{\partial x}\frac{\partial w}{\partial y} + \frac{\partial w}{\partial x}\frac{\partial w_0}{\partial y} + \frac{\partial w_0}{\partial x}\frac{\partial w}{\partial y}, \tag{6}$$

$$k_x = -\frac{\partial^2 w}{\partial x^2}, \tag{7}$$

$$k_y = -\frac{\partial^2 w}{\partial y^2}, \tag{8}$$

$$k_{xy} = -2\frac{\partial^2 w}{\partial x \partial y}. \tag{9}$$

These expressions are in general accurate enough for moderately large vibrations of plates.

2.1. Elastic strain energy

The elastic strain energy U_P of a rectangular isotropic plate, under Kirchhoff's hypothesis $\sigma_{zz} = \tau_{zx} = \tau_{zy} = 0$, is given by Ref. [1]

$$U_P = \frac{1}{2}\int_0^a \int_0^b \int_{-h/2}^{h/2} [\sigma_x(\varepsilon_x - \alpha\Delta T) + \sigma_y(\varepsilon_y - \alpha\Delta T) + \tau_{xy}\gamma_{xy}]\,\mathrm{d}x\,\mathrm{d}y\,\mathrm{d}z, \tag{10}$$

where α is the coefficient of thermal expansion and ΔT (Kelvin) is the temperature variation (assumed to be not uniform along the plate thickness) with respect to a reference temperature; σ_{xx}, σ_{yy} and τ_{xy} are the Kirchhoff stresses; and ε_{xx}, ε_{yy} and γ_{xy} are Green's strains. Eq. (10) is valid within the limit of elasticity of the plate's material and for moderately large displacements; therefore it is suitable in the context of the present nonlinear study. The simplicity of Eq. (10) is due to the Lagrangian description of the plate, which allows integration over the plate in the original undeformed configuration. The Kirchhoff stresses for a homogeneous and isotropic material (case of plane stress) are given by Ref. [1]

$$\begin{Bmatrix} \sigma_x \\ \sigma_y \\ \tau_{xy} \end{Bmatrix} = \begin{bmatrix} \dfrac{E}{1-\nu^2} & \dfrac{\nu E}{1-\nu^2} & 0 \\ \dfrac{\nu E}{1-\nu^2} & \dfrac{E}{1-\nu^2} & 0 \\ 0 & 0 & \dfrac{E}{2(1+\nu)} \end{bmatrix} \left(\begin{Bmatrix} \varepsilon_x \\ \varepsilon_y \\ \gamma_{xy} \end{Bmatrix} - \begin{Bmatrix} 1 \\ 1 \\ 0 \end{Bmatrix} \alpha\Delta T \right). \tag{11}$$

By using Eqs. (1–3,10,11), the following expression is obtained for uniform thickness:

$$\begin{aligned} U_P = {} & \frac{1}{2}\frac{Eh}{1-\nu^2}\int_0^a \int_0^b \left(\varepsilon_{x,0}^2 + \varepsilon_{y,0}^2 + 2\nu\varepsilon_{x,0}\varepsilon_{y,0} + \frac{1-\nu}{2}\gamma_{xy,0}^2\right)\mathrm{d}x\,\mathrm{d}y \\ & + \frac{1}{2}\frac{Eh^3}{12(1-\nu^2)}\int_0^a \int_0^b \left(k_x^2 + k_y^2 + 2\nu k_x k_y + \frac{1-\nu}{2}k_{xy}^2\right)\mathrm{d}x\,\mathrm{d}y \\ & - \alpha\frac{E}{1-\nu}\int_0^a \int_0^b \int_{-h/2}^{h/2} \Delta T[\varepsilon_{x,0} + \varepsilon_{y,0} + z(k_x + k_y)]\,\mathrm{d}x\,\mathrm{d}y\,\mathrm{d}z, \end{aligned} \tag{12}$$

where the first term, on the right-hand side, is the membrane (also referred to as stretching) energy, the second one is the bending energy and the third term is due to thermal effects. It is now assumed that the thermal distribution is constant along x and y, and is linear along z, i.e.

$$\Delta T = \Delta T_0 + \Delta T_1 z/h, \tag{13}$$

where ΔT_0 is the thermal variation of the middle surface of the plate, and the external surfaces of the plate have temperature variations $\Delta T_0 - \Delta T_1/2$ and $\Delta T_0 + \Delta T_1/2$, respectively.

Under the assumption (13), the last of the three integrals on the right-hand side of Eq. (12) can be integrated on z giving

$$-\alpha\frac{Eh}{1-\nu}\int_0^a\int_0^b \Delta T_0(\varepsilon_{x,0}+\varepsilon_{y,0})\,\mathrm{d}x\,\mathrm{d}y-\alpha\frac{Eh^2}{12(1-\nu)}\int_0^a\int_0^b \Delta T_1(k_x+k_y)\,\mathrm{d}x\,\mathrm{d}y. \tag{14}$$

Eq. (14) shows that for similar thermal variations ΔT_0 and ΔT_1 and similar strain and change in curvature, the second term is smaller than the first one by the factor $h/12$, which is small for thin plates. Eqs. (12) and (14) can be written as a function of the middle-surface displacements u, v, w by using Eqs. (4)–(9). Since Eqs. (4)–(6) present linear and nonlinear terms in w, Eq. (14) introduces both linear and quadratic terms in the plate displacements in Eq. (12). In particular, ΔT_0 introduces in-plane strains and ΔT_1 introduces bending strains.

2.2. Boundary conditions and solution

The kinetic energy T_P of a rectangular plate, by neglecting rotary inertia, is given by

$$T_\mathrm{P}=\frac{1}{2}\rho_\mathrm{P}h\int_0^a\int_0^b(\dot{u}^2+\dot{v}^2+\dot{w}^2)\,\mathrm{d}x\,\mathrm{d}y, \tag{15}$$

where ρ_p is the mass density of the plate. In Eq. (6) the overdot denotes a time derivative.

The virtual work W done by the external forces is written as

$$W=\int_0^a\int_0^b(q_x u+q_y v+q_z w)\,\mathrm{d}x\,\mathrm{d}y, \tag{16}$$

where q_x, q_y and q_z are the distributed forces per unit area acting in x, y and z directions, respectively. In the present study, only a single harmonic force orthogonal to the plate is considered; therefore $q_x=q_y=0$. The external distributed load q_z applied to the plate, due to the concentrated force $\tilde{f}$, is given by

$$q_z=\tilde{f}\delta(y-\tilde{y})\,\delta(x-\tilde{x})\,\cos(\omega t), \tag{17}$$

where ω is the excitation frequency, t is the time, δ is the Dirac delta function, $\tilde{f}$ is the force magnitude positive in z direction; $\tilde{x}$ and $\tilde{y}$ give the position of the point of application of the force.

Plates with fixed edges are considered because they are highly sensitive to thermal variations since they cannot expand. The following boundary conditions are introduced for plates with fixed edges:

$$u=v=w=w_0=0,\quad M_x=\mp k\partial w/\partial x\quad \text{at } x=0,\ a, \tag{18a–e}$$

$$u=v=w=w_0=0,\quad M_y=\mp k\partial w/\partial y\quad \text{at } y=0,\ b, \tag{19a–e}$$

where k is the stiffness per unit length of the elastic, distributed rotational springs placed at the four edges, $x=0$, a and $y=0$, b; the minus sign in Eqs. (18e) and (19e) applies at the boundaries $x=0$ and $y=0$. Eqs. (18e) and (19e) represent the case of an elastic rotational constraint at the shell edges. They give any rotational constraint from zero bending moment ($M_x=0$ and $M_y=0$, unconstrained rotation, obtained for $k=0$) to perfectly clamped plate ($\partial w/\partial x=0$ and $\partial w/\partial y=0$, obtained as limit for $k\to\infty$), according to the value of k.

The displacements u, v and w are expanded by using the following expressions, which satisfy identically the geometric boundary conditions (18a–c) and (19a–c):

$$u(x,y,t)=\sum_{m=1}^{M}\sum_{n=1}^{N}u_{2m,n}(t)\,\sin(2m\pi x/a)\,\sin(n\pi y/b), \tag{20a}$$

$$v(x,y,t)=\sum_{m=1}^{M}\sum_{n=1}^{N}v_{m,2n}(t)\,\sin(m\pi x/a)\,\sin(2n\pi y/b), \tag{20b}$$

$$w(x,y,t)=\sum_{m=1}^{\hat{M}}\sum_{n=1}^{\hat{N}} w_{m,n}(t)\,\sin(m\pi x/a)\,\sin(n\pi y/b), \tag{20c}$$

where m and n are the numbers of half-waves in x and y directions, respectively, and t is the time; $u_{m,n}(t)$, $v_{m,n}(t)$ and $w_{m,n}(t)$ are the generalized coordinates, which are unknown functions of t. M and N indicate the terms necessary in the expansion of the in-plane displacements and, in general, are larger than $\hat{M}$ and $\hat{N}$, respectively, which indicate the terms in the expansion of w.

On the other hand, Eqs. (18e) and (19e) can be rewritten in the following form:

$$M_x=\frac{Eh^3}{12(1-\nu^2)}(k_x+\nu k_y)=\mp k\frac{\partial w}{\partial x}\quad \text{at } x=0,\ a, \tag{21}$$

$$M_y=\frac{Eh^3}{12(1-\nu^2)}(k_y+\nu k_x)=\mp k\frac{\partial w}{\partial y}\quad \text{at } y=0,\ b. \tag{22}$$

If k is different from zero, an additional potential energy stored by the elastic rotational springs at the plate edges must be added. This potential energy U_R is given by

$$U_R=\frac{1}{2}\int_0^b k\left\{\left[\left(\frac{\partial w}{\partial x}\right)_{x=0}\right]^2+\left[\left(\frac{\partial w}{\partial x}\right)_{x=a}\right]^2\right\}\mathrm{d}y+\frac{1}{2}\int_0^a k\left\{\left[\left(\frac{\partial w}{\partial y}\right)_{y=0}\right]^2+\left[\left(\frac{\partial w}{\partial y}\right)_{y=b}\right]^2\right\}\mathrm{d}x. \tag{23}$$

In order to simulate clamped edges in numerical calculations, a very high value of the stiffness k must be assumed. This approach is usually referred to as the artificial spring method [1], which can be regarded as a variant of the classical penalty method. The values of the spring stiffness simulating a clamped plate can be obtained by studying the convergence of the natural frequencies of the linearized solution by increasing the value of k. In fact, it was found that the natural frequencies of the system converge asymptotically with those of a clamped plate when k becomes very large.

Initial geometric imperfections of the rectangular plate are considered only in z direction. They are associated with zero initial stress. The imperfection w_0 is expanded in the same form of w, i.e. in a double Fourier sine series satisfying the boundary conditions (18d) and (19d) at the plate edges

$$w_0(x,y)=\sum_{m=1}^{\tilde{M}}\sum_{n=1}^{\tilde{N}} A_{m,n}\sin(m\pi x/a)\,\sin(n\pi y/b), \tag{24}$$

where $A_{m,n}$ are the modal amplitudes of imperfections; $\tilde{N}$ and $\tilde{M}$ are integers indicating the number of terms in the expansion.

2.3. Lagrange equations of motion

The non-conservative damping forces are assumed to be of viscous type and are taken into account by using the Rayleigh's dissipation function

$$F=\frac{1}{2}c\int_0^a\int_0^b(\dot{u}^2+\dot{v}^2+\dot{w}^2)\,\mathrm{d}x\,\mathrm{d}y, \tag{25}$$

where c has a different value for each term of the mode expansion. Simple calculations give

$$F=\frac{1}{2}(ab/4)\left[\sum_{n=1}^{\hat{N}}\sum_{m=1}^{\hat{M}} c_{m,n}\dot{w}_{m,n}^2+\sum_{n=1}^{N}\sum_{m=1}^{M} c_{m,n}\dot{u}_{m,n}^2+\sum_{n=1}^{N}\sum_{m=1}^{M} c_{m,n}\dot{v}_{m,n}^2\right]. \tag{26}$$

The damping coefficient $c_{m,n}$ is related to modal damping ratio (in this case it is a damping ratio of the generalized coordinate), that can be evaluated from experiments, by $\varsigma_{m,n}=c_{m,n}/(2\mu_{m,n}\omega_{m,n})$, where $\omega_{m,n}$ is the natural circular frequency of mode (m, n) and $\mu_{m,n}$ is the mass associated with this generalized coordinate, given by $\mu_{m,n}=\rho_s h(ab/4)$.

The following notation is introduced for brevity

$$\mathbf{q} = \{u_{m,n}, v_{m,n}, w_{m,n}\}^{\mathrm{T}}, \quad m = 1, \ldots M \text{ or } \hat{M} \text{ and } n = 1, \ldots N \text{ or } \hat{N}. \tag{27}$$

The generic element of the time-dependent vector $\mathbf{q}$ is referred to as q_j, which is the generalized coordinate; the dimension of $\mathbf{q}$ is dofs, which is the number of degrees of freedom used in the mode expansion.

The generalized forces Q_j are obtained by differentiation of the Rayleigh's dissipation function and of the virtual work done by external forces

$$Q_j = -\frac{\partial F}{\partial \dot{q}_j} + \frac{\partial W}{\partial q_j}. \tag{28}$$

The Lagrange equations of motion are

$$\frac{\mathrm{d}}{\mathrm{d}t}\left(\frac{\partial T_{\mathrm{P}}}{\partial \dot{q}_j}\right) - \frac{\partial T_{\mathrm{P}}}{\partial q_j} + \frac{\partial U}{\partial q_j} = Q_j, \quad j = 1, \ldots \text{dofs}, \tag{29}$$

where $\partial T_{\mathrm{P}}/\partial q_j = 0$ and the potential energy is given by $U = U_{\mathrm{P}} + U_{\mathrm{R}}$, where U_{P} is given by Eq. (12) and U_{R} by Eq. (23). These second-order equations have very long expressions containing quadratic and cubic nonlinear terms. In particular, the only term containing nonlinearities is

$$\frac{\partial U}{\partial q_j} = \sum_{k=1}^{\text{dofs}} f_{k,j} q_k + \sum_{i,k=1}^{\text{dofs}} f_{i,k,j} q_i q_k + \sum_{i,k,l=1}^{\text{dofs}} f_{i,k,l,j} q_i q_k q_l, \tag{30}$$

where coefficients f have long expressions that include also geometric imperfections and thermal variations. Quadratic nonlinearities of the type ${q_i}^2$ (in particular for $q_i = w_{m,n}$) are never present in the equations of motion of perfect flat plates without thermal variation. This is a difference with respect to curved panels and it is physically explained by the fact that no different displacement is observed for flat plates in z and $-z$ directions, due to the symmetry. Presence of quadratic nonlinearities is the reason for significant asymmetric displacement in z and $-z$ that is observed in the results of this study presented in the following sections in case of initial geometric imperfections or initial thermal buckling. In fact, thermal variations can cause buckling of the plate, which may result in an initial buckled configuration (no more flat) also in case of plates without any initial imperfection. Also in this case, quadratic nonlinearities arise in the equations of motion due to the initial buckled deformation. It can be observed that the presence of quadratic nonlinearities associated to initial geometric imperfection changes the thermal buckling behaviour of the plate destroying the pitchfork bifurcation and giving a continuous buckling behaviour, as shown in the following section.

Numerical results show that, for very thin plates, geometric imperfections of the magnitude of the plate thickness give quadratic terms with an effect of the same order of cubic terms, for vibration amplitude of the order of the plate thickness. Therefore the classical hardening-type nonlinearity, which is characteristics of flat plates, is transformed by significant imperfections and thermal variations into softening-type nonlinearity, turning to hardening-type only for larger vibration amplitudes.

3. Numerical results

The equations of motion have been obtained by using the *Mathematica* computer software [34] in order to perform analytical surface integrals of trigonometric functions (e.g. integrals in Eq. (5)). The generic j-th Lagrange equation is divided by the modal mass associated with $\ddot{q}_j$ and then is transformed in two first-order equations. A non-dimensionalization of variables is also performed for computational convenience: the frequencies are divided by the natural radian frequency $\omega_{m,n}$ of the mode (m, n) investigated, and the vibration amplitudes are divided by the plate thickness h. The resulting $2 \times$ dofs equations are studied by using (i) the software AUTO 97 [35] for continuation and bifurcation analysis of nonlinear ordinary differential equations and (ii) direct integration of the equations of motion by using the DIVPAG routine of the Fortran library IMSL. The software AUTO 97 is capable of continuation of the solution, bifurcation analysis and branch switching by using pseudo-arclength continuation [1] and collocation methods. In particular, the plate response under harmonic excitation has been studied by using an analysis in three steps: (i) for zero excitation,

the temperature variation is used as bifurcation parameter; the solution has been started at zero thermal variation where the solution is the trivial undisturbed configuration of the plate and has been continued up to reach the desired magnitude of the thermal variation; (ii) then, the excitation frequency has been fixed far enough from resonance and the magnitude of the excitation has been used as bifurcation parameter; the solution has been continued using as restarting point the deformed configuration obtained at step (i); and (iii) when the desired magnitude of excitation has been reached, the solution has been continued by using the excitation frequency as bifurcation parameter.

Initially a numerical test has been performed in order to study the convergence of the buckling temperature parameter $\lambda_T = 1000\alpha\Delta T_0$ for the square isotropic clamped plate under uniform temperature variation studied by Gossard et al. [36] and by Liew et al. [37] and having the following dimensions and material properties: $a = b = 0.1\,\text{m}$, $h = 0.001\,\text{m}$, $E = 198 \times 10^9\,\text{Pa}$, $\rho = 7850\,\text{kg/m}^3$, $\nu = 0.3$ and $\alpha = 2 \times 10^{-6}\,\text{K}^{-1}$. Results are reported in Table 1 and show convergence of the present model to the results in Refs. [36] and [37].

Then, calculations have been performed for a rectangular AISI 304 stainless steel plate, see Fig. 1, with the following dimensions and material properties: $a = 0.25\,\text{m}$, $b = 0.24\,\text{m}$, $h = 0.00027\,\text{m}$, $E = 198 \times 10^9\,\text{Pa}$, $\rho = 7850\,\text{kg/m}^3$, $\nu = 0.3$ and $\alpha = 17.3 \times 10^{-6}\,\text{K}^{-1}$. This plate has fundamental mode ($n = 1$, $m = 1$) with radian frequency $\omega_{1,1} = 44.4 \times 2\pi\,\text{rad/s}$ for clamped edges simulated with $k = 10^5\,\text{N/rad}$. The plate is considered for harmonic excitation around the fundamental resonance, at the plate centre (at $x = a/2$ and $y = b/2$), of magnitude $\tilde{f} = 0.042\,\text{N}$, assuming modal damping $\zeta_{1,1} = 0.012$ (the same damping ratio is assumed for all the generalized coordinates). Present results have been obtained by using a model with 39 dofs, i.e. with 39 generalized coordinates. In particular, they are: $w_{1,1}$, $w_{3,1}$, $w_{5,1}$, $w_{7,1}$, $w_{1,3}$, $w_{3,3}$, $w_{5,3}$, $w_{7,3}$, $w_{1,5}$, $w_{3,5}$, $w_{5,5}$, $w_{1,7}$, $w_{3,7}$, $u_{2,1}$, $u_{4,1}$, $u_{6,1}$, $u_{8,1}$, $u_{2,3}$, $u_{4,3}$, $u_{6,3}$, $u_{8,3}$, $u_{2,5}$, $u_{4,5}$, $u_{6,5}$, $u_{2,7}$, $u_{4,7}$, $v_{1,2}$, $v_{3,2}$, $v_{5,2}$, $v_{7,2}$, $v_{1,4}$, $v_{3,4}$, $v_{5,4}$, $v_{7,4}$, $v_{1,6}$, $v_{3,6}$, $v_{5,6}$, $v_{1,8}$, $v_{3,8}$.

Table 1
Convergence of the buckling temperature parameter $\lambda_T = 1000\alpha\Delta T_0$ for the isotropic clamped plate studied by Gossard et al. [36] and by Liew et al. [37]

39 dofs	63 dofs	107 dofs	Ref. [36]	Ref. [37]
0.375	0.36	0.34	0.337	0.333

Fig. 1. Photo of the stainless steel thin rectangular plate fixed to a thick frame with a traditional exciter (shaker) and laser spot at the centre of the plate.

The thermal postbuckling behaviour of the plate subjected to uniform temperature variation is shown in Fig. 2 and shows buckling through a supercritical pitchfork bifurcation for temperature variation $\Delta T_0 = 0.26\,\mathrm{K}$. Branch 2 is arising from the bifurcation point and is associated with plate deflection (in Fig. 2 the plate deflection at the centre is shown). Therefore, very small increase of the plate temperature with respect to the

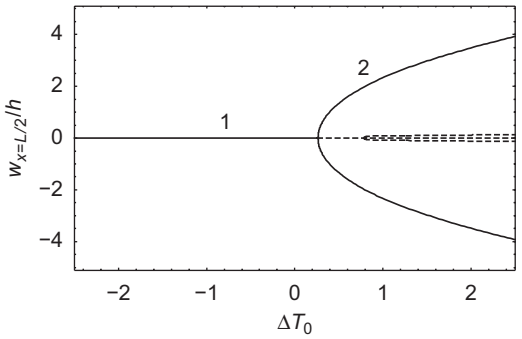

Fig. 2. Thermal postbuckling of the perfect plate under uniform temperature variation. ——, stable solution; - -, unstable solution.

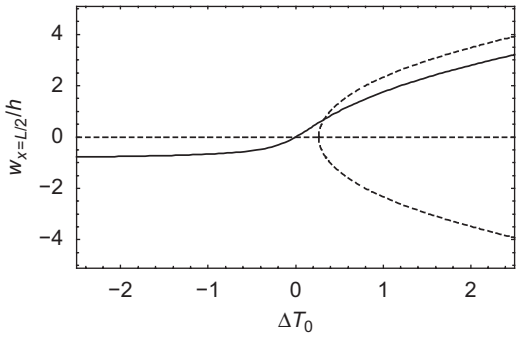

Fig. 3. Thermal postbuckling of the plate with initial geometric imperfection under uniform temperature variation. ——, plate with initial imperfection $A_{1,1} = h$; - -, perfect plate.

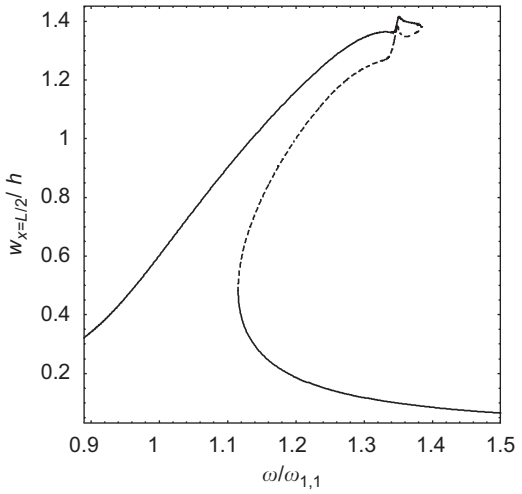

Fig. 4. Frequency-response curve at the centre of the perfect plate; excitation at the centre with $\tilde{f} = 0.042\,\mathrm{N}$ in the frequency neighbourhood of the first resonance; results show the first harmonic only; $\zeta_{1,1} = 0.012$; 39 dofs.—, stable solution; - -, unstable solution.

clamping frame cause buckling. On branch 1 the plate has no deflection. In particular, a positive variation ΔT_0 generates plate compression while a negative variation ΔT_0 gives traction with an increase of the natural frequency.

Fig. 3 shows the effect of geometric imperfection $A_{1,1} = h$ with the same shape of the fundamental mode (1,1) and amplitude equal to the plate thickness. The bifurcation is destroyed by the geometric imperfection and the behaviour is continuous. A deflection increasing the initial curvature due to imperfection is obtained for a positive variation ΔT_0, while the plate is reducing curvature and deflection for a negative variation ΔT_0.

In case of linear temperature variation through the plate thickness ΔT_1, no bifurcation is obtained also for the perfect plate, but a deflection arises growing with ΔT_1; anyway, this deflection is very small since the studied plate is very thin and h is a small number of the order of 10^{-4}, as already discussed after Eq. (14). In particular, a variation ΔT_1 of the order of 100 K gives a negligible deflection in the present case.

The maximum plate oscillation at the centre of the perfect plate is presented in Fig. 4 for harmonic excitation of 0.042 N applied at the centre of the plate in the frequency neighbourhood of the fundamental

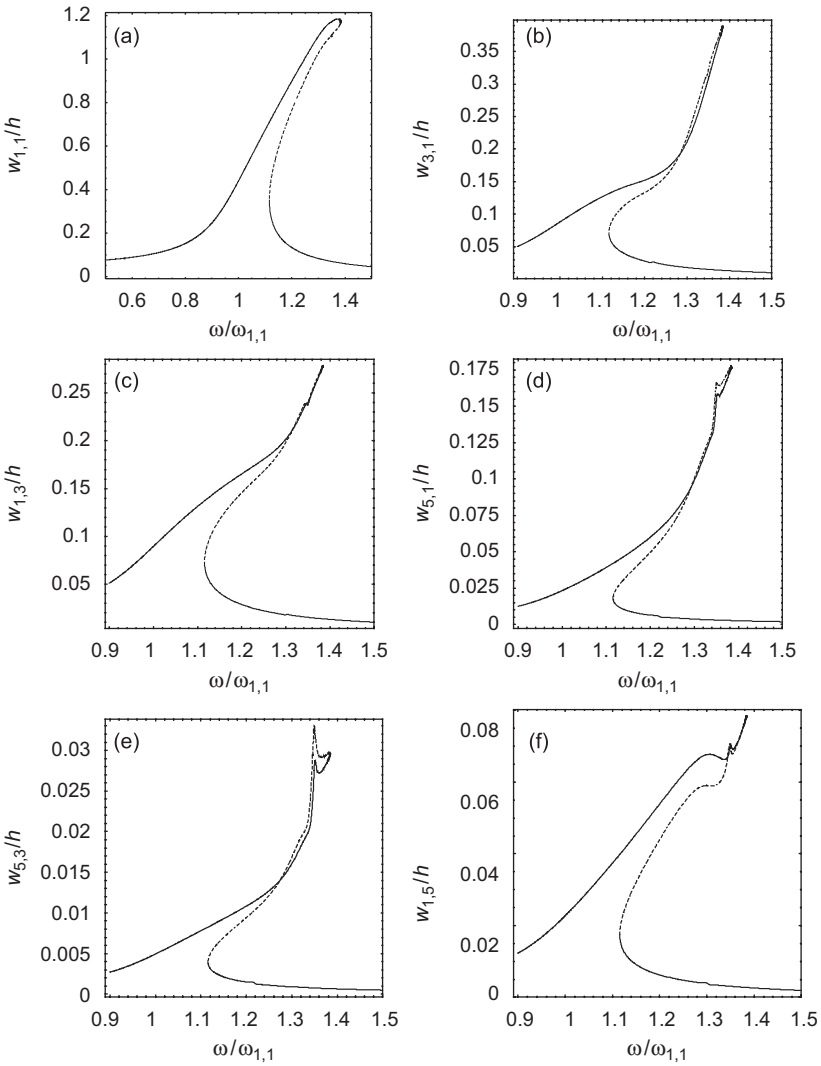

Fig. 5. Frequency-response behaviour of the perfect plate; $A_{1,1} = 0$, $\tilde{f} = 0.042$ N and $\zeta_{1,1} = 0.012$; 39 dofs. ——, stable periodic response; - -, unstable periodic response. (a) Maximum of the generalized coordinate $w_{1,1}$; (b) maximum of the generalized coordinate $w_{3,1}$; (c) maximum of the generalized coordinate $w_{1,3}$; (d) maximum of the generalized coordinate $w_{5,1}$; (e) maximum of the generalized coordinate $w_{5,3}$; and (f) maximum of the generalized coordinate $w_{1,5}$.

mode; modal damping $\zeta_{1,1} = 0.012$ is assumed for all the generalized coordinates. It is evident that the clamped boundary condition gives strong hardening-type nonlinearity. The strange behaviour near the response peak is due to two 3:1 internal resonances: (i) between mode (1,1) and (3,1) for $\omega = 1.215 \times \omega_{1,1}$ and (ii) between mode (1,1) and (1,3) for $\omega = 1.3 \times \omega_{1,1}$. The contributions of the most significant generalized coordinates to the response shown in Fig. 4 are plotted in Fig. 5.

Geometric imperfection $A_{1,1} = 0.91h$ with the same shape of the fundamental mode completely changes the plate nonlinear response, as shown in Fig. 6. In fact, the response initially shows a softening-type nonlinearity, turning to hardening nonlinearity for vibration amplitude around $0.8h$. Results in Fig. 6 are non-dimensionalized in frequency dividing by the natural frequency $\omega_{1,1}$ of the perfect plate; in particular, the natural frequency of the plate with imperfection is about $1.3 \times \omega_{1,1}$ in this case. A 1/2 subharmonic response is also shown in Fig. 6 around $0.65 \times \omega_{1,1}$.

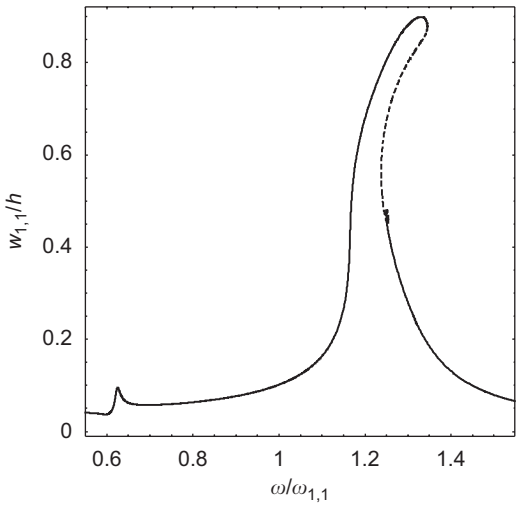

Fig. 6. Response of the plate with imperfections around the first resonance; $A_{1,1} = 0.91h$, $\tilde{f} = 0.042$ N and $\zeta_{1,1} = 0.012$; 39 dofs. ——, stable periodic response; - -, unstable periodic response.

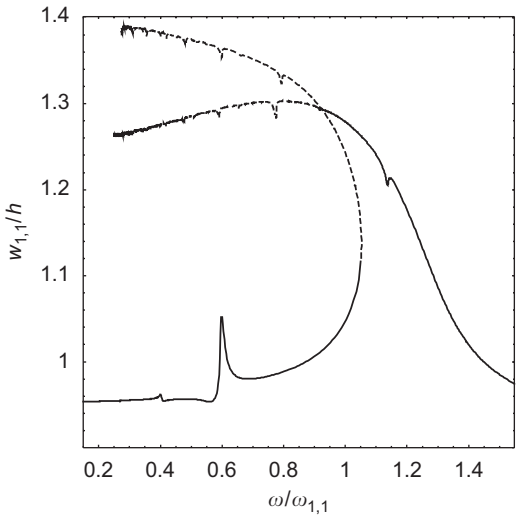

Fig. 7. Frequency-response curve of the perfect plate in presence of uniform temperature variation $\Delta T_0 = 0.481$ K, $\tilde{f} = 0.042$ N and $\zeta_{1,1} = 0.012$; 39 dofs. ——, stable periodic response; - -, unstable periodic response.

The nonlinear response of the perfect plate with a positive temperature variation $\Delta T_0 = 0.481$ K is shown in Fig. 7. This value of ΔT_0 has been chosen since it gives an initial deflection due to thermal buckling with the same amplitude of the initial imperfection $0.91h$ used in Fig. 6. The nonlinear response is of the softening type and the amplitude is largely reduced with respect to the two previous cases (the ordinate starts at amplitude $0.9h$ in Fig. 7 differently from other figures). Results in Fig. 7 are non-dimensionalized in frequency dividing by the natural frequency $\omega_{1,1}$ of the perfect plate under no temperature variation; in particular, the natural frequency of the thermally buckled plate is about $1.2 \times \omega_{1,1}$ in this case. A 1/2 subharmonic response is also shown in Fig. 7 around $0.6 \times \omega_{1,1}$.

The nonlinear response in presence of both temperature variation $\Delta T_0 = 0.25$ K and geometric imperfection $A_{1,1} = 0.5h$, giving an initial deflection around $0.91h$ used in Figs. 6 and 7, is shown in Fig. 8. The response, see Fig. 8a, is initially strongly softening, becoming strongly hardening for vibration amplitude around $0.8h$.

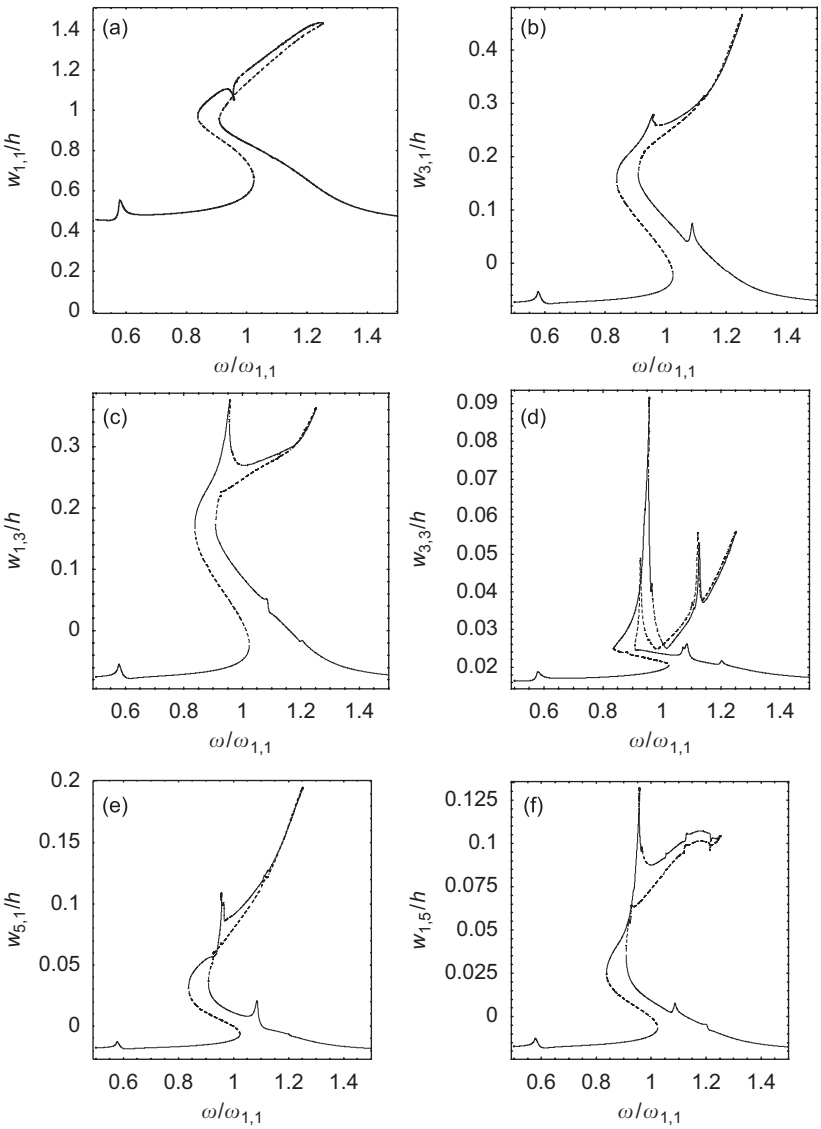

Fig. 8. Frequency-response curve of the plate with imperfections in presence of uniform temperature variation $\Delta T_0 = 0.25$ K, $A_{1,1} = 0.5h$, $\tilde{f} = 0.042$ N and $\zeta_{1,1} = 0.012$; 39 dofs. ——, stable periodic response; - -, unstable periodic response. (a) Maximum of the generalized coordinate $w_{1,1}$; (b) maximum of the generalized coordinate $w_{3,1}$; (c) maximum of the generalized coordinate $w_{1,3}$; (d) maximum of the generalized coordinate $w_{3,3}$; (e) maximum of the generalized coordinate $w_{5,1}$; and (f) maximum of the generalized coordinate $w_{1,5}$.

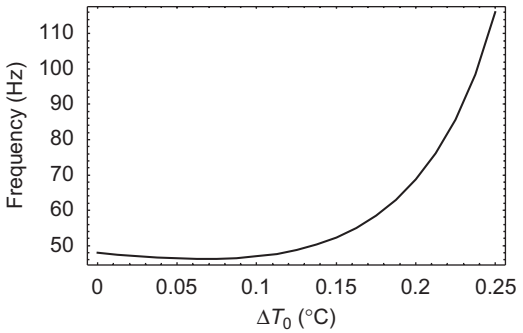

Fig. 9. Effect of uniform temperature variation ΔT_0 on the natural frequency of the fundamental mode (1,1) of the plate with geometric imperfection $A_{1,1} = 0.5h$; 39 dofs.

Qualitatively the response is similar to the one shown in Fig. 6 for the plate with initial imperfection, but the nonlinear behaviour is strongly enhanced. Fig. 8 shows the six principal generalized coordinates; 2:1 internal resonances among mode (1,1) with (1,3) and (3,1) are detected, as well as 3:1 internal resonance between mode (1,1) and mode (3,3).

Fig. 9 gives the natural frequency of the fundamental mode (1,1) of the plate with geometric imperfection $A_{1,1} = 0.5h$ versus the temperature variation ΔT_0; the results in this figure have been obtained by linearizing the static equilibrium equation involving temperature.

4. Experimental results

Tests have been conducted on two stainless steel plates, plates A and B; plate A has the same dimensions and material properties used in Section 3 for numerical calculations ($a = 0.25\,\text{m}$, $b = 0.24\,\text{m}$, $h = 0.00027\,\text{m}$, $E = 198 \times 10^9\,\text{Pa}$, $\rho = 7850\,\text{kg/m}^3$, $\nu = 0.3$ and $\alpha = 17.3 \times 10^{-6}\,\text{K}^{-1}$); on the other hand, plate B has only one difference: increased thickness $h = 0.5\,\text{mm}$. Each plate was practically clamped to a AISI 410 stainless steel rectangular frame, see Fig. 1, having coefficient of thermal expansion $\alpha_F = 9.9 \times 10^{-6}\,\text{K}^{-1}$.

The plates have been subjected to (i) burst-random excitation to identify the natural frequencies and perform a modal analysis by measuring the plate response on a grid of points, (ii) harmonic excitation, increasing or decreasing by very small steps the excitation frequency in the spectral neighbourhood of the lowest natural frequencies, to characterize nonlinear responses in presence of large-amplitude vibrations (step-sine excitation). The excitation has been provided by a self-constructed electromagnetic exciter that transmit the excitation force to the plate by mean of a rare-earth permanent magnet without contact, as shown in Fig. 10. The reason for using this device is that it minimizes higher harmonics in the excitation. A piezoelectric miniature force transducer B&K 8203 of the weight of 3.2 g, glued to the plate and connected to the magnet, measured the force transmitted. The plate response has been measured by using a very accurate laser Doppler vibrometer by Polytec (sensor head OFV-505 and controller OFV-5000) in order to have non-contact measurement without introduction of inertia. The time responses have been measured by using the Difa Scadas II front-end, connected to a HP c3000 workstation, and the software CADA-X 3.5b of LMS for signal processing, data analysis, experimental modal analysis and excitation control. The same front-end has been used to generate the excitation signal. The CADA-X closed-loop control has been used to keep constant the value of the excitation force for any excitation frequency, during the measurement of the nonlinear response.

Geometric imperfections of the plates have been detected by using a Matsushita ANR 1282 laser triangulation sensor to measure the actual plate surface.

4.1. Nonlinear results for plate A

The contour plot indicating the deviation from the ideal panel surface is reported in Fig. 11. In particular, Fig. 11a presents the shape of the plate during the following nonlinear tests, while Fig. 11b shows the second

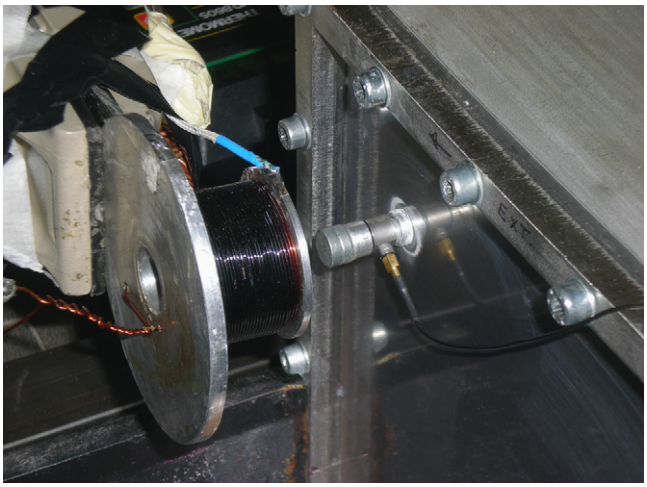

Fig. 10. Non-contact excitation system with rare-earth permanent magnet.

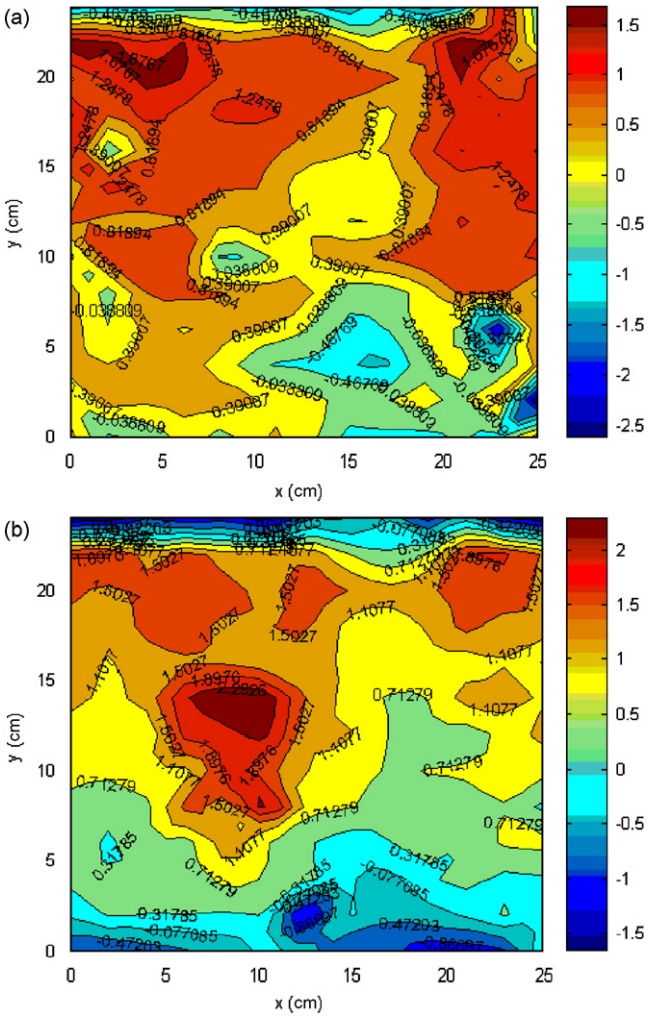

Fig. 11. Contour plot indicating measured geometric imperfections as deviation from the flat surface. Deviations are in millimetres; $h = 0.27$ mm. (a) Tested equilibrium position and (b) second equilibrium position.

equilibrium position of the plate (e.g. see Fig. 2 to observe the two coexisting equilibrium positions of the buckled plate). Geometric imperfections are always present in actual plates. In the present case, imperfection presents a complex shape and are very different from the first natural mode (1,1). Actually in the tested plates these imperfections are associated to initial stresses. These initial stresses are not measured and are not taken into account in the modelling since the tested plate is extremely thin so the locked-in initial bending stresses are negligible with respect to the effect of imperfections and in-plane initial stresses are minimized by the experimental set-up. Geometric imperfections shown in Fig. 11 are very large, being several times the plate thickness, since the plate is very thin (0.27 mm) and presents an initial curvature due to lamination.

Fig. 12 shows the measured oscillation (displacement, directly measured by using the Polytec laser Doppler vibrometer with displacement decoder DD-200 in the OFV-5000 controller; measurement position at the centre of the panel) around the fundamental frequency, i.e. mode (1, 1), versus the excitation frequency for three different force levels: 0.1, 0.2, and 0.3 N. The excitation point was at $\tilde{x} = a/6$ and $\tilde{y} = b/6$. The natural (linear) frequency is identified at 48.6 Hz at beginning of the nonlinear tests, but it varies with the temperature.

The closed-loop control used in the experiments keeps constant the amplitude of the harmonic excitation force, after filtering the signal from the load cell in order to use only the harmonic component with the given excitation frequency. The measured oscillation reported in Fig. 12 has been filtered in order to eliminate any frequency except the excitation frequency (first harmonic of the response). Experiments have been performed increasing and decreasing the excitation frequency (up and down); the frequency step used in this case is 0.05 Hz, 16 periods have been measured with 128 points per period and 40 periods have been waited before data acquisition every time that the frequency is changed. The hysteresis between the two curves (up = increasing frequency; down = decreasing frequency) is clearly visible for all the three excitation levels. Sudden increments (jumps) of the vibration amplitude are observed when increasing and decreasing the excitation frequency; these indicate softening-type nonlinearity, which is due to the initial imperfection and the temperature variation. In fact, Fig. 12 can be favourably compared to Fig. 7, which is for a perfect plate under uniform temperature variation. In particular, the vibration amplitude larger than h shows amplitude modulations, as shown in Fig. 13 for the time response at the peak of the curve for excitation 3 N. Table 2 gives the temperatures of the plate and the frame at assembly and during the nonlinear tests. In particular, practically the plate and the frame have the same temperature during experiments. However, an increment of

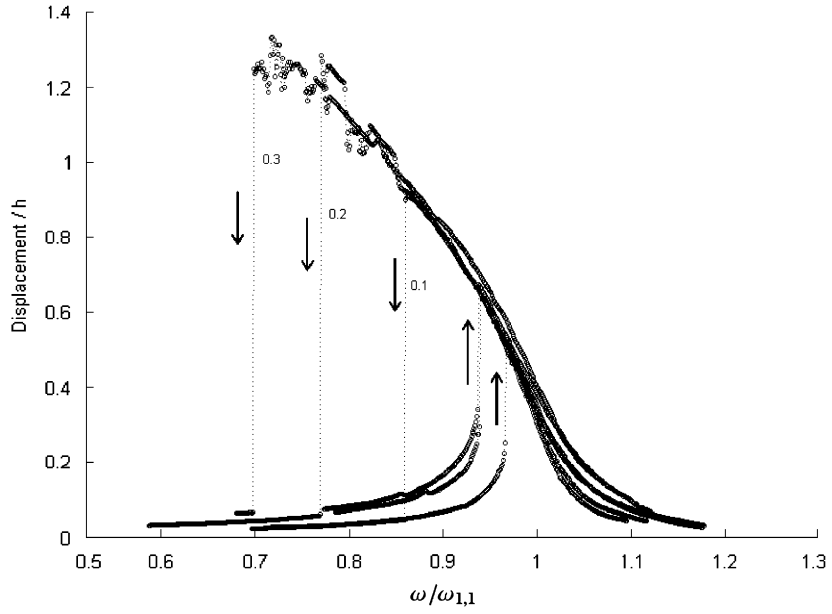

Fig. 12. Experimental non-dimensional oscillatory displacement (peak) versus non-dimensional excitation frequency for different excitation (0.1, 0.2, and 0.3 N) measured at $x = a/6$, $y = b/6$; $h = 0.27$ mm; mode (1,1). ○, experimental point; - -, connecting line; →, direction of movement along the line.

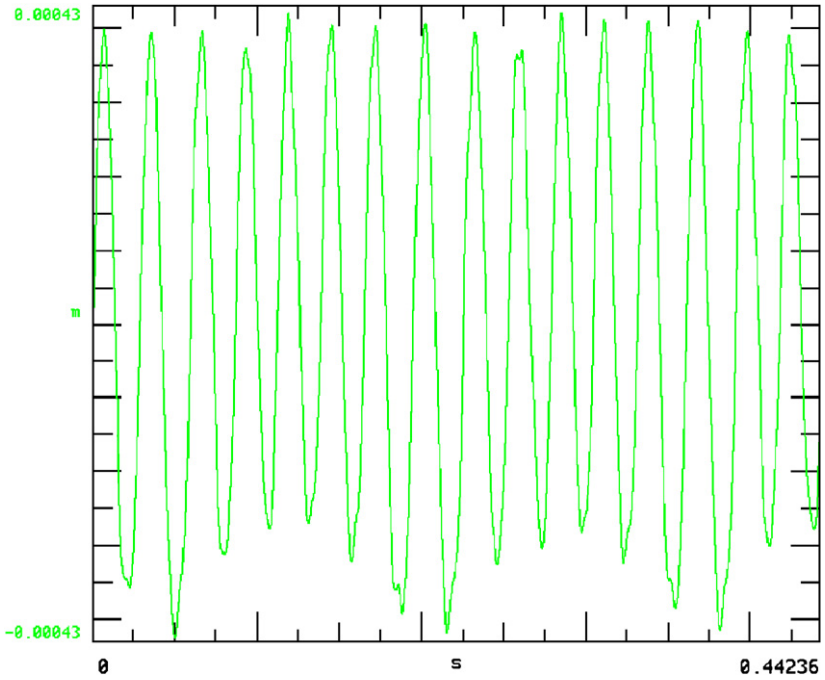

Fig. 13. Experimental time response for excitation frequency $\omega/\omega_{1,1} = 0.7$ (36.15 Hz), excitation force 0.3 N, $h = 0.27$ mm.

Table 2
Temperatures (°C) of the plate, T_P, and of the frame, T_F, during nonlinear experiments

	Assembly	0.1 up	0.1 down	0.2 up	0.2 down	0.3 up	0.3 down
T_P	21.0	21.1	21.2	21.4	21.7	22.7	22.8
T_F	20.7	20.9	21.2	21.4	21.7	22.7	22.8

Plate A.

1.8 °C is observed between the initial condition and the temperature measured during the last experiment for excitation 0.3 N decreasing the excitation frequency (down). This increase of temperature is due to the electronic equipments and amplifiers used during the experiments that produce heating.

Fig. 2 is for a perfect plate clamped to a fixed frame. Since the frame presents a coefficient of thermal expansion $\alpha_F = 9.9 \times 10^{-6}\,\mathrm{K}^{-1}$, this must be subtracted to the coefficient $\alpha = 17.3 \times 10^{-6}\,\mathrm{K}^{-1}$ of the plate. Therefore, the temperature scale in Fig. 2 must be multiplied by 2.338 in order to obtain the uniform temperature variation in case of the plate fixed to the thermally expansible frame used in the experiments. The buckling thermal load is increased from 0.26 K to about 0.61 K.

It must be observed that the force input around resonance was only partially distorted with respect to the imposed pure sinusoidal excitation. This is due to the non-contact excitation, which minimizes higher-order harmonics. Fig. 14 shows the harmonic components in the excitation signal for 0.3 N in the frequency range investigated. In particular, the second harmonic is always relatively small, while the most problematic is the fourth harmonic of the excitation signal; anyway, it reaches amplitudes always smaller than the first harmonic itself, which is the only one controlled.

4.2. Nonlinear results for plate B

The thermal postbuckling behaviour of plate B subjected to uniform temperature variation is shown in Fig. 15 and shows buckling through a supercritical pitchfork bifurcation for temperature variation

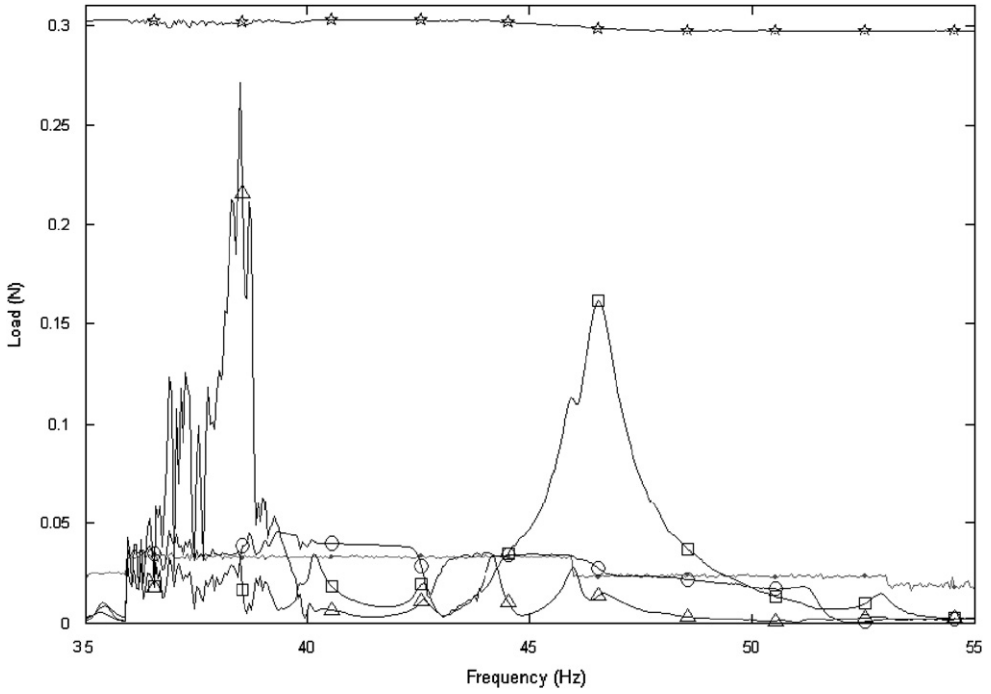

Fig. 14. Harmonic components of the excitation force for the 3 N level, $h = 0.27$ mm; mode (1,1). ● = mean value; ☆ = first harmonic; ○ = second harmonic; □ = third harmonic; △ = fourth harmonic.

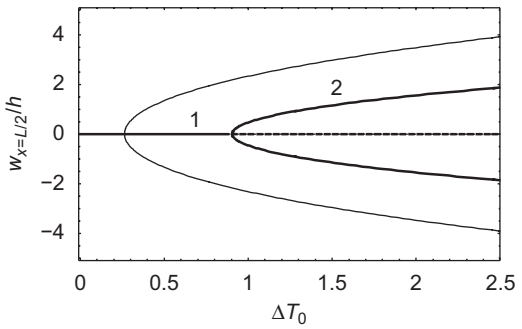

Fig. 15. Thermal postbuckling of the perfect plate under uniform temperature variation. Thin line, $h = 0.27$ mm; thick line, $h = 0.5$ mm. ——, stable solution; - -, unstable solution.

$\Delta T_0 = 0.9$ K. In Fig. 15 comparison with results for plate A are also shown and show a largely decreased temperature effect with the thickness increase from 0.27 to 0.5 mm. Also in this case, the temperature scale in Fig. 15 must be multiplied by 2.338 in order to obtain the uniform temperature variation in case of the plate fixed to the thermally expansible frame used in the experiments. Therefore, the buckling thermal load is increased from 0.9 K to about 2.1 K.

The measured geometric imperfection of plate B is shown in Fig. 16. Maximum deviation from the flat surface is of amplitude around half thickness, which can be considered moderate. The geometry of the imperfection is not far from the first mode (1,1). The plate presented only one stable equilibrium position, differently from plate A.

Fig. 17 shows the measured oscillation (displacement, directly measured by using the Polytec laser Doppler vibrometer at the centre of the panel) around the fundamental frequency, i.e. mode (1, 1), versus the excitation frequency for four different force levels: 0.35, 0.45, 0.55 and 0.9 N. The excitation point was at $\tilde{x} = a/6$ and

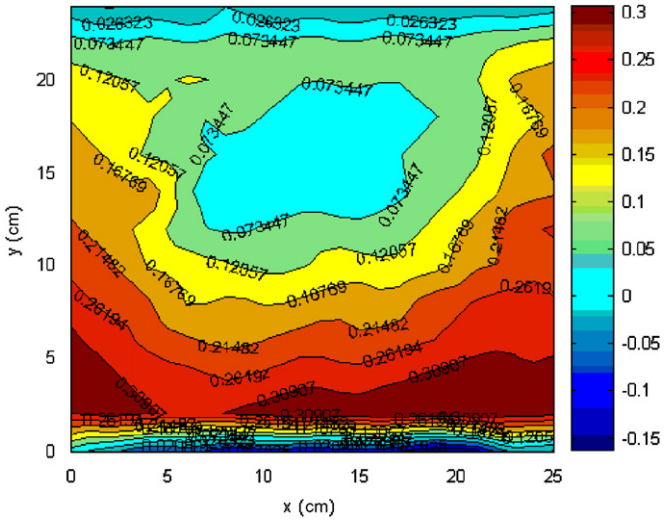

Fig. 16. Contour plot indicating measured geometric imperfections as deviation from the flat surface. Deviations are in millimetres; $h = 0.5$ mm.

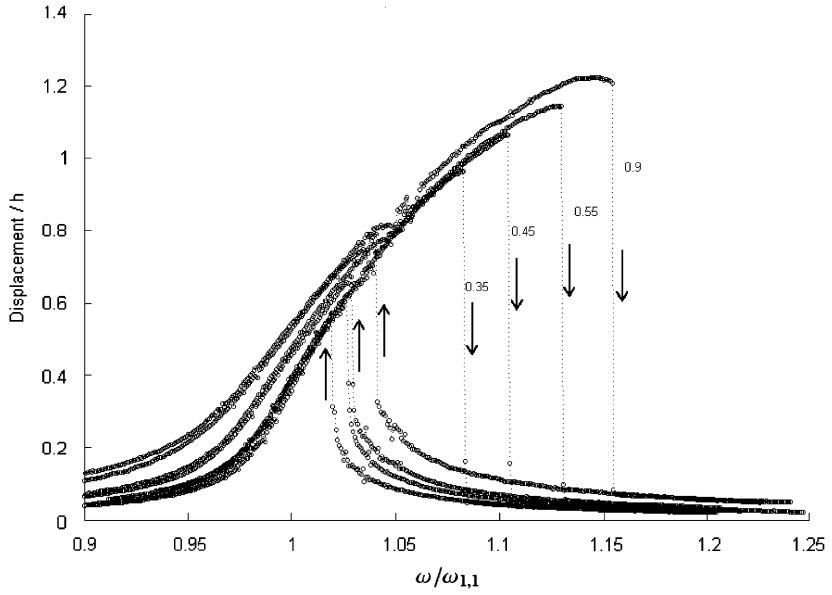

Fig. 17. Experimental non-dimensional oscillatory displacement (peak) versus non-dimensional excitation frequency for different excitation (0.35, 0.45, 0.55, and 0.9 N) measured at $x = a/6$, $y = b/6$; $h = 0.5$ mm; mode (1,1). ○, experimental point; - -, connecting line; →, direction of movement along the line.

$\tilde{y} = b/6$. The natural (linear) frequency is identified at 66.0 Hz at beginning of the nonlinear tests, but it slightly varies with the temperature. The measured oscillation reported in Fig. 17 has been filtered in order to eliminate any frequency except the excitation frequency. Experiments have been performed increasing and decreasing the excitation frequency (up and down) with the same parameters used for plate A. The hysteresis between the two curves (up = increasing frequency; down = decreasing frequency) is clearly visible for all the four excitation levels. Differently from plate A, a hardening nonlinearity is detected for plate B. In fact, plate B presents moderate geometric imperfection and the temperature variation plays a much smaller role,

Table 3
Temperatures (°C) of the plate, T_P, and of the frame, T_F, during nonlinear experiments

	Assembly	0.35 up	0.35 down	0.45 up	0.45 down	0.55 up	0.55 down	0.9 up	0.9 down
T_P	21.0	21.1	21.1	21.1	21.2	21.3	21.5	21.5	21.7
T_F	20.5	21.0	21.1	21.1	21.2	21.3	21.5	21.5	21.7

Plate B.

as shown Fig. 15. Fig. 17 can be favourably compared to Fig. 4, which is for a perfect plate without temperature variation, but it presents a reduced nonlinearity due to initial imperfection and temperature variation. Table 3 gives the temperatures of the plate and the frame at assembly and during the nonlinear tests. Also in this case, the plate and the frame present practically the same temperature, and the maximum temperature variation is about 2 K, i.e. very similar to what observed for plate A.

5. Conclusions

Calculations and experiments show that nonlinear vibration of very thin clamped plates is largely affected by temperature variations of the order of 1 °C. Actually this value gives plate buckling for the plate A tested experimentally. The effect of temperature variation decreases with plate thickness. Also geometric imperfections, measured as deviation from the ideal flat surface, play a fundamental role in predicting the nonlinear response. Imperfections are usually larger for very thin plates, as shown in the experimental case. Therefore, both temperature variations and geometric imperfections must be taken into account in many applications to calculate nonlinear vibrations of thin plates with fixed or clamped edges. In fact, the classical hardening type nonlinearity characteristic of flat rectangular plates can be transformed into a softening type nonlinearity by temperature variations and geometric imperfections.

References

[1] M. Amabili, *Nonlinear Vibrations and Stability of Shells and Plates*, Cambridge University Press, New York, USA, 2008.
[2] C.-Y. Chia, *Nonlinear Analysis of Plates*, McGraw-Hill, New York, USA, 1980.
[3] M. Sathyamoorthy, Nonlinear vibration analysis of plates: a review and survey of current developments, *Applied Mechanics Reviews* 40 (1987) 1553–1561.
[4] C.-Y. Chia, Geometrically nonlinear behavior of composite plates: a review, *Applied Mechanics Reviews* 41 (1988) 439–451.
[5] H.-N. Chu, G. Herrmann, Influence of large amplitude on free flexural vibrations of rectangular elastic plates, *Journal of Applied Mechanics* 23 (1956) 532–540.
[6] J.N. Reddy, Geometrically nonlinear transient analysis of laminated composite plates, *AIAA Journal* 21 (1983) 621–629.
[7] M. Ganapathi, T.K. Varadan, B.S. Sarma, Nonlinear flexural vibrations of laminated orthotropic plates, *Computers and Structures* 39 (1991) 685–688.
[8] W. Han, M. Petyt, Geometrically nonlinear vibration analysis of thin, rectangular plates using the hierarchical finite element method–II: 1st mode of laminated plates and higher modes of isotropic and laminated plates, *Computers and Structures* 63 (1997) 309–318.
[9] P. Ribeiro, M. Petyt, Geometrical non-linear, steady-state, forced, periodic vibration of plate, part I: model and convergence study, *Journal of Sound and Vibration* 226 (1999) 955–983.
[10] P. Ribeiro, M. Petyt, Geometrical non-linear, steady-state, forced, periodic vibration of plate, part II: stability study and analysis of multi-modal response, *Journal of Sound and Vibration* 226 (1999) 985–1010.
[11] P. Ribeiro, M. Petyt, Non-linear free vibration of isotropic plates with internal resonance, *International Journal of Non-Linear Mechanics* 35 (2000) 263–278.
[12] C.-S. Chen, J.R. Hwang, J.L. Doong, Nonlinear vibration of an initially stressed plate based on a modified plate theory, *International Journal of Solids and Structures* 38 (2001) 8563–8583.
[13] M. Amabili, Nonlinear vibrations of rectangular plates with different boundary conditions: theory and experiments, *Computers and Structures* 82 (2004) 2587–2605.
[14] M. Amabili, Theory and experiments for large-amplitude vibrations of rectangular plates with geometric imperfections, *Journal of Sound and Vibration* 291 (2006) 539–565.
[15] B. Harras, R. Benamar, R.G. White, Geometrically non-linear free vibration of fully clamped symmetrically laminated rectangular composite plates, *Journal of Sound and Vibration* 251 (2002) 579–619.

[16] M. El Kadiri, R. Benamar, Improvement of the semi-analytical method based on Hamilton's principle and spectral analysis, for determination of the geometrically non-linear response of thin straight structures, part III: steady state periodic forced response of rectangular plates, *Journal of Sound and Vibration* 264 (2003) 1–35.
[17] N. Yamaki, K. Otomo, M. Chiba, Non-linear vibrations of a clamped circular plate with initial deflection and initial edge displacement, part I: theory, *Journal of Sound and Vibration* 79 (1981) 23–42.
[18] N. Yamaki, K. Otomo, M. Chiba, Non-linear vibrations of a clamped circular plate with initial deflection and initial edge displacement, part II: experiment, *Journal of Sound and Vibration* 79 (1981) 43–59.
[19] C. Touzé, O. Thomas, A. Chaigne, Asymmetric non-linear forced vibrations of free-edge circular plates, part 1: theory, *Journal of Sound and Vibration* 258 (2002) 649–676.
[20] J. Girish, L.S. Ramachandra, Thermal postbuckled vibrations of symmetrically laminated composite plates with initial geometric imperfections, *Journal of Sound and Vibration* 282 (2005) 1137–1153.
[21] S.J. Lee, J.N. Reddy, Non-linear response of laminated composite plates under thermomechanical loading, *International Journal of Non-linear Mechanics* 40 (2005) 971–985.
[22] P. Ribeiro, Thermally induced transitions to chaos in plate vibrations, *Journal of Sound and Vibration* 299 (2007) 314–330.
[23] P. Ribeiro, E. Jansen, Non-linear vibrations of laminated cylindrical shallow shells under thermomechanical loading, *Journal of Sound and Vibration* 315 (2008) 626–640.
[24] L. Librescu, W. Lin, Non-linear response of laminated plates and shells to thermomechanical loading: implications of violation of interlaminar shear traction continuity requirement, *International Journal of Solids and Structures* 36 (1999) 4111–4147.
[25] G.N. Praveen, J.N. Reddy, Nonlinear transient thermoelastic analysis of functionally graded ceramic-metal plates, *International Journal of Solids and Structures* 35 (1998) 4457–4476.
[26] J. Yang, S. Kitipornchai, K.M. Liew, Large amplitude vibration of thermo-electro-mechanically stressed FGM laminated plates, *Computer Methods in Applied Mechanics and Engineering* 192 (2003) 3861–3885.
[27] X.-L. Huang, H.-S. Shen, Nonlinear vibration and dynamic response of functionally graded plates in thermal environments, *International Journal of Solids and Structures* 41 (2004) 2403–2427.
[28] J.-S. Park, J.-H. Kim, Thermal postbuckling and vibration analyses of functionally graded plates, *Journal of Sound and Vibration* 289 (2006) 77–93.
[29] J. Woo, S.A. Meguid, L.S. Ong, Nonlinear free vibration behaviour of functionally graded plates, *Journal of Sound and Vibration* 289 (2006) 595–611.
[30] A. Allahverdizadeh, M.H. Naei, M. Nikkhah Bahrami, Vibration amplitude and thermal effects on the nonlinear behaviour of thin circular functionally graded plates, *International Journal of Mechanical Sciences* 50 (2008) 445–454.
[31] N. Sundararajan, T. Prakash, M. Ganapathi, Nonlinear free flexural vibrations of functionally graded rectangular and skew plates under thermal environments, *Finite Elements in Analysis and Design* 42 (2005) 152–168.
[32] E. Manoach, P. Ribeiro, Coupled, thermoelastic, large amplitude vibrations of Timoshenko beams, *International Journal of Mechanical Sciences* 46 (2004) 1589–1606.
[33] M. Amabili, S. Farhadi, Shear deformable versus classical theories for nonlinear vibrations of rectangular isotropic and laminated composite plates, *Journal of Sound and Vibration*, 2008, in press, doi:10.1016/j.jsv.2008.08.006.
[34] S. Wolfram, *The Mathematica Book*, fourth ed, Cambridge University Press, Cambridge, UK, 1999.
[35] E.J. Doedel, A.R. Champneys, T.F. Fairgrieve, Y.A. Kuznetsov, B. Sandstede, X. Wang, *AUTO 97: continuation and bifurcation software for ordinary differential equations (with homcont)*, Concordia University, Montreal, Canada, 1998.
[36] M.L. Gossard, P. Seide, W.M. Roberts, Thermal buckling of plates, NACA TN 2771, USA, 1952.
[37] K.M. Liew, J. Yang, S. Kitipornchai, Postbuckling of piezoelectric FGM plates subject to thermo-electro-mechanical loading, *International Journal of Solids and Structures* 40 (2003) 3869–3892.